ORIGINAL PAPER

Synthesis and Catalytic Activity of Cu(II), Fe(III) and Bi(III) Complexes of Thio-Schiff Base Encapsulated in Zeolite-Y for Hydroxylation of Phenol

Hanna S. Abbo · Salam J. J. Titinchi

Abstract Coordination of 4-{[(1*E*)-(2-hydroxyphenyl) methylene]amino}-2,4-dihydro-3*H*-1,2,4-triazole-3-thione, [sal(thiotriazol)], with M-exchanged zeolite-Y (M = Cu(II), Fe(III) and Bi(III)) leads to the encapsulation of the metal complexes in the supercages of zeolite-Y by flexible ligand method. The prepared encapsulated metal complexes have been characterized by physico-chemical techniques, which indicated that the complexes were effectively encapsulated inside the supercages of Na–Y, without any modification of the morphology and structure of the zeolite. 3D model structure generated for these complexes suggests that zeolite-Y can accommodate these complexes in the FAU supercages without any strain. The catalytic activity of all the catalysts towards the hydroxylation of phenol was evaluated under heterogeneous conditions using hydrogen peroxide as an oxidant. Under the optimized conditions, these catalysts show moderate activity with excellent selectivity (>95%) towards catechol. These catalysts were stable in hydroxylation of phenol and have been reused a further three times after recovering. The results reflect the reusability of the catalysts, as no significant loss in their catalytic activity was noticed.

Keywords Zeolite-Y · Encapsulation ·
Triazole thione-Schiff base · Phenol hydroxylation

H. S. Abbo
Department of Chemistry, University of the Western Cape,
Private Bag X17, Bellville, Cape Town 7535, South Africa

S. J. J. Titinchi (✉)
Department of Chemistry, University of the Western Cape,
Private Bag X17, Bellville, Cape Town 7535, South Africa
e-mail: stitinchi@uwc.ac.za

1 Introduction

Zeolites are well-defined and ordered structures with systematic nano-cavities, which are ideal matrices for hosting nano-sized transition metal complexes, which are of great interest for catalytic applications [1–5].

Modern catalytic science faces challenging problems connected with the urgent necessity to create new highly effective industrial processes, which are selective, ecologically pure and consume minimum energy. At least creating organised molecular systems, which are designed to have an optimum space arrangement and energy and orbital correspondence of the catalytic system components and substrates, can solve some of these problems.

Immobilization of homogeneous metal complexes inside the supercages of zeolites either by encapsulation or grafting techniques [2, 4, 6–10] enhance their activity/ selectivity compared to the corresponding neat complexes as well as thermal stability and reusability.

Encapsulation of homogeneous metal based catalyst in the supercages of zeolite matrix is a field of continuing interest; it considers as new environment friendly approach for performing chemical reactions [11–13]. These materials possess the advantages of both homogeneous as well as heterogeneous catalysts [14–17]. While the disadvantages of heterogeneous catalysts are mechanisms hard to determine and reaction rates are often limited. Therefore, the search for new oxidation heterogeneous catalysts is one of the most essential current topics for both industrial and academic research.

Direct hydroxylation of phenol is one of the most important oxidation reactions. The production of dihydroxybenzenes with hydrogen peroxide through an environmentally-friendly catalytic process is desirable. Amongst the different oxidants used in oxidation catalysis,

hydrogen peroxide is ideally suitable due to its low cost and generates no hazardous by-products during the reaction.

Numerous works on phenol hydroxylation have extensively studied using various Schiff base transition metal complexes encapsulated in zeolite-Y [11–13]. Selective oxidation of phenol at mild conditions with eco-friendly oxidant (H_2O_2) is still a challenging area in catalysis research.

As a continuation of research on catalyzed hydroxylation of phenol [18–25], the present work describes the synthesis and physicochemical characterization of the encapsulated Cu(II), Fe(III) and Bi(III) complexes of 2,4-dihydro-4-[(2-hydroxyphenyl)-methylene]amino]-3H-1,2,4-triazole-3-thione ligand, abbreviated as [sal(thiotriazol)], in zeolite-Y. To the best of our knowledge, this is a first report on using thio-Schiff base complexes encapsulated in the supercages of zeolite-Y for phenol hydroxylation. The dimensions of the optimized coordination geometry of the encapsulated metal complexes were calculated using 3D modeling to confirm that the metal complexes is confined within the dimension of the zeolite cages and cannot escape out of the cage after encapsulation.

The encapsulated complexes have been screened as heterogeneous catalysts for hydroxylation of phenol with hydrogen peroxide as the oxygen donor. The effect of different experimental parameters such as reaction temperature, time, amount of catalyst, solvent type, and volume and phenol/H_2O_2 molar ratios on the catalytic conversion was also investigated in order to optimize the reaction conditions for maximum transformation of phenol as well as better selectivity for the formation of catechol.

2 Experimental

2.1 Materials

Hydrazine hydrate (99%), carbon disulphide, formic acid (85%), salicylaldehyde, copper (II) nitrate, iron (III) nitrate and bismuth (III) nitrate, phenol, acetic acid, acetonitrile and carbon tetrachloride were from Aldrich. Zeolite Na–Y was purchased from Fluka.

2.2 Physical Measurements and Analysis

The elemental analyses were performed at University of Cape Town, South Africa. The percentage metal contents of the encapsulated complexes were determined by Inductively Coupled Plasma Atomic Emission Spectrometry (ICP-AES) at the University of Stellenbosch, Cape Town, South Africa. ^{1}H NMR spectra were recorded in $CDCl_3$ using a Varian XR200 spectrometer. Sample signals

are relative to the resonance of residual protons on carbons in the solvent. The nitrogen adsorption/desorption and BET surface area was determined at −196 °C using a Tristar 3000 micromeritics. All samples were degassed prior to the measurement at 120 °C for 13 h. The ATR-IR measurements were carried out on a Perkin-Elmer Spectrum 100 FTIR spectrometer. Electronic spectra were recorded on a GBC UV/VIS 920 UV–Visible spectrophotometer in absolute ethanol or in Nujol (by layering the mull of the sample to the inside of one of the cuvette while keeping another one layered with Nujol as reference). Scanning Electron Micrographs (SEM) of the catalysts were recorded on Hitachi X-650 EM. The samples were dusted on alumina and coated with a thin film of gold to prevent surface changing and to protect the surface material from thermal damage by the electron beam. In all analyses, a uniform thickness of about 0.1 mm was maintained. Powder X-ray diffraction (XRD) was recorded by Bruker AXS D8 Advance, high-resolution diffractometer with Cu K_α radiation ($\lambda = 1.5406$ Å) fitted with PSD Vantec gas detector, at iThemba Labs, Cape Town, South Africa.

All catalyzed reaction products were analyzed using a Varian CP3800 gas chromatograph fitted with flame ionization detector. A HP-PONA capillary column (50 m × 0.35 mm (id) × 0.5 μm film thickness, Agilent technologies, J&W Scientific) and Star workstation computer software were used. The retention time of all peaks was compared with authentic samples and also the identity of the products was further confirmed by a GC–MS using Finnigan MAT GCQ GC/Mass spectrometer.

2.3 Preparations of the Encapsulated Complexes

The Schiff base [sal(thiotriazol)] ligand was prepared starting from hydrazine (Scheme 1), followed by encapsulation which was achieved by: (i) ion exchange of M^{n+} in NaY zeolite and (ii) coordination of the intrazeolite metal ion with the [sal(thiotriazol)] ligand.

2.3.1 Preparation of the Ligand

The ligand was synthesized as following (Scheme 1):

i. Thiocarbohydrazide was synthesized according to the reported procedure [26].
ii. 4-Amino-2,4-dihydro-1,2,4-triazole-5-thione was synthesized according to a reported method [27] with slight modification.
iii. 4-{[(1E)-(2-hydroxyphenyl)methylene]amino}-2,4-dihydro-3H-1,2,4-triazole-3-thione.

Equimolar quantities of salicylaldehyde (1.22 g, 0.01 mol) and [sal(thiotriazol)] Schiff base (1.16 g, 0.01 mol) dissolved in methanol (20 mL). Several drops of

Scheme 1 Synthetic route of
the ligand [sal(thiotriazol)]
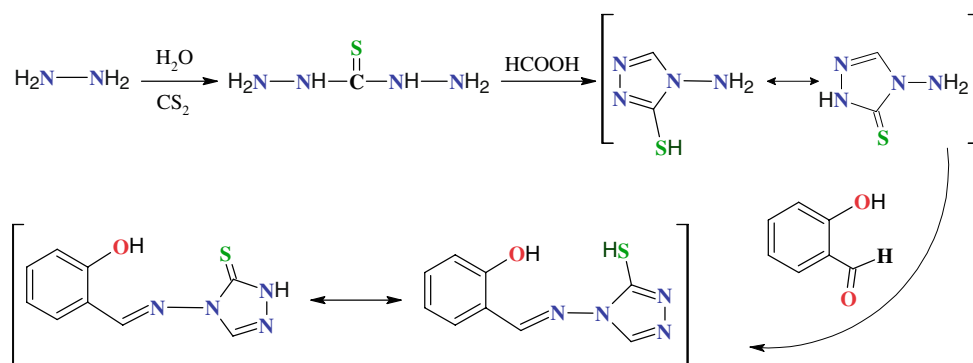
concentrated sulphuric acid were added to the solution and refluxed for 3 h. The solid obtained was filtered and recrystallized from ethanol to afford pale yellow crystals.

2.3.2 Preparation of Metal Exchanged Zeolite, M–Y

The ion-exchanged Na–Y zeolites were prepared by a standard ion-exchange procedure by exchanging Na ions of Na–Y (5.0 g suspended in 300 mL deionized water) with 50 mmol aqueous nitrate solutions of the corresponding metal cations (Cu(II), Fe(III) or Bi(III)). The mixture was stirred at 90 °C for 24 h, filtered, washed with copious amount of hot deionised water followed by Soxhlet extraction with acetonitrile for 1 h till the filtrate was free from any metal ion content. The resulting precipitate was dried at 150 °C in air for 24 h.

2.3.3 Preparation of Zeolite-Y Encapsulated Metal Complexes

The encapsulated complexes were prepared following the general flexible ligand method [28, 29]. An amount of 1.0 g M–Y and 2.5 g of the ligand [sal(thiotriazol)] were mixed in a 50 mL MeCN. The suspension mixture was refluxed and stirred overnight. After cooling, the slurry was subjected to Soxhlet extraction in acetonitrile for 48 h to remove excess uncomplexed ligand that remained in the cavities of the zeolite as well as any free metal complex located on the surface of the zeolite. The uncomplexed metal ions present in the zeolite were removed by exchanging back encapsulated zeolite ML_2-Y with aqueous 0.01 M NaCl solution. The encapsulated complexes were filtered, washed with copious amount of hot distilled water till the filtered was free from chloride. The solids obtained were dried at 150 °C for several hours to constant weight.

2.4 Catalytic Liquid Phase Hydroxylation

Oxidation of phenol using the prepared catalysts was carried out in 50 mL glass parallel reactor vessels (Radley's Discovery Technologies 12 place Heated Carousel

Reaction Station fitted with a Reflux unit). In a typical reaction, phenol (4.7 g, 0.05 mol) and 30% solution of H_2O_2 (5.67 g, 0.05 mol) were mixed in 2 mL of the desired solvent and the reaction mixture was heated at 80 °C with continuous stirring. Toluene was added as internal standard. Requisite amount of catalyst (0.010 g) was added to the reaction mixture, and this was assumed as the starting point of the reaction. The progress of the reaction was monitored by GC analysis using an internal standard technique. The reaction products were analyzed using a gas chromatograph and monitored at set time intervals by withdrawing small aliquots. Samples were filtered before analysis. The oxidation products were identified by comparison with authentic samples and GC–Mass data.

3 Results and Discussion

3.1 Syntheses and Characterisation of Catalysts

The [sal(thiotriazol)] ligand was synthesised starting from hydrazine (Scheme 1). Thiocarbohydrazide was then reacted with glacial acetic acid to form the *N*-amino-1,2,4-triazol thione, followed by Schiff base condensation with salicylaldehyde.

The synthesized ligand [sal(thiotriazol)] was encapsulated in the nano-cavities of zeolite-Y by flexible ligand method, which involves the reaction of ion-exchanged Y-zeolite with excess of acetonitrile solution of the ligand. The solvent (acetonitrile) facilitated the insertion of ligand in the cavity of the zeolite due to its flexible nature. The ligand with the dimension of less than the zeolite pore openings of 7.4 Å diffused through the zeolite supercages followed by complexation with metal ions. Complexation of the ligand with Cu(II) and Fe(III) ion-exchanged zeolite was accompanied by the colour change (pale green and pale orange, respectively), while encapsulated Bi(III) complex was colourless.

The crude mass was subjected to Soxhlet extraction in acetonitrile to remove excess ligand that remained uncomplexed in the cavities of the zeolite as well as

located on the surface of the zeolite along with free complex, if any. The uncomplexed metal ions from the zeolite were removed by exchanging back [M[sal(thiotriazol)]₂]-Y with aqueous 0.01 M NaCl solution. Thus, the percentage of metal content estimated by ICP is only due to encapsulation of the complex in the supercages of the zeolite-Y. The encapsulated catalysts were further characterized by FT-IR and electronic spectra and X-ray powder diffraction patterns (vide infra), which support the encapsulation of metal complexes inside the cavities of the zeolite. Neat complexes have also been prepared (Titinchi and Abbo, unpublished results) for comparison with encapsulated complexes.

Zeolite Na–Y is the host starting material with the unit cell composition of $Na_{48}(SiO_2)_{144}(AlO_2)_{48}$ xH_2O. The chemical composition was obtained by combination of data from elemental analyses, ICP and energy-dispersive X-ray spectroscopy (EDX) analysis of several crystalline parts of the sample and the average was taken. The chemical analyses of the encapsulated complexes (Table 1) revealed the presence of organic moiety with C/N ratio almost similar to that of the neat complexes. The M/N ratio suggesting 2:1 ligand to metal stoichiometry analogous to the model complexes with formula $[CuL_2(H_2O)_2]$, $[FeL_2(H_2O)Cl]$ and $[BiL_2Cl]$. The Si/Al ratio of the encapsulated complexes was similar to parent Na–Y zeolite, which indicates no change in zeolite framework after encapsulation.

As the encapsulated complexes were purified well by Soxhlet extraction with acetonitrile, the metal and element contents found after encapsulation are only due to the presence of the metal complexes in the cavity of the zeolite-Y.

These catalysts are also well characterized by IR spectroscopy (Fig. 1). The metal exchange zeolites exhibit bands around 1140, 1035, 960, 780 and 740 cm^{-1} due to the zeolite framework. No significant broadening or shift of the structure-sensitive zeolite vibrations at 1130 cm^{-1} (due to the asymmetric T–O stretch) on ion-exchange and upon encapsulation of the complexes indicates that there is no defect of zeolite framework or dealumination and the matrix remains unchanged during the process, in agreement with XRD results.

The intensities of the absorption peaks in the encapsulated complexes are low due to their low concentration in zeolite matrix and only detected in the region where

Table 1 Chemical analysis of the samples

Zeolite samples	C/N	M/N	Si/Al	M (wt%)
Na–Y	–	–	3.00	–
CuL₂(H₂O)₂-Y	1.87	0.52	2.99	2.31
FeL₂(H₂O)Cl-Y	1.91	0.50	3.03	0.51
BiL₂Cl-Y	1.86	1.83	2.89	0.85
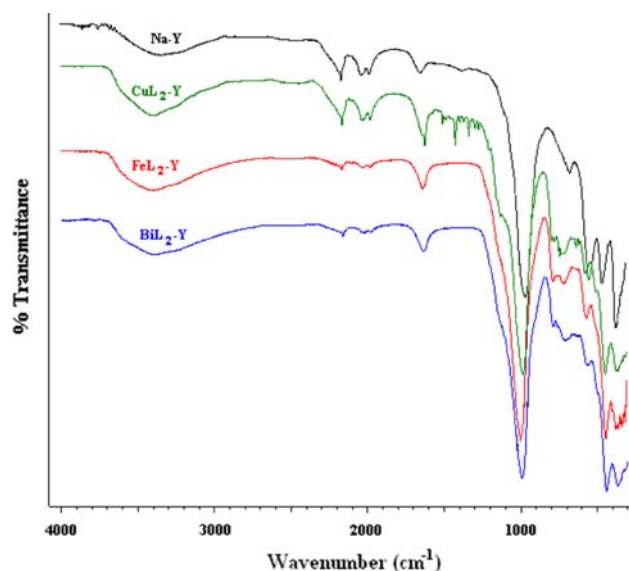
Fig. 1 FT-IR spectral pattern of Na–zeolite-Y and the encapsulated catalysts

typically the Na–Y does not absorb, specifically in the regions 1600–1200 and 350–450 cm^{-1}.

IR spectrum of the ligand [sal(thiotriazol)] shows characteristic bands at 3132, 2715 and at ∼1110 cm^{-1}, which are assigned to v(N–H), v(S–H) and v(C=S) respectively [30]. These observations suggest that the Schiff base exhibits thiol–thione tautomerism (Scheme 1), which is well-known with all of the other members of this family of triazoles [31–34].

The band at 3332 cm^{-1} observed in the ligand due to phenolic OH disappeared in complexes. This indicates the ligand coordinated to the metal ion through phenolic oxygen atom via deprotonation. A strong band at 1623 cm^{-1} in the ligand assigned to v(C=N) lowered by (10–15) cm^{-1} on complexation due to the coordination of the azomethine nitrogen with the metal ion.

The bands due to C=S and S–H vibrations of the ligand remained unperturbed in these complexes indicating that the metal is not coordinated through sulphur atom [35]. These observations suggest the non-involvement of sulfur atom in coordination.

A broad band appeared in the region 3400–3520 cm^{-1} in all complexes indicating the presence of coordinated water and two weaker bands in the region 750–800 and 700–720 cm^{-1} [30, 36].
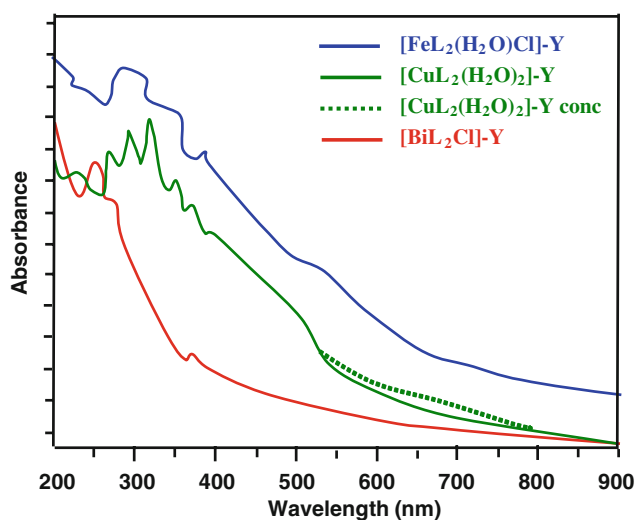
The appearance of new moderately intense bands in the low frequency region of 350–500 cm^{-1} in all the complexes are assigned to stretching frequencies of v(M–O) and v(M–N) bonds. It further indicates the coordination of nitrogen and oxygen to the metal. Fe and Bi-based catalysts exhibits a band in the region 320–325 cm^{-1} assigned to vM–Cl [37].

On the basis of IR data, it is concluded that all the metal ions are coordinated to the azomethine nitrogen, phenolic oxygen, and water molecule or/and chloride.

It is worthy mentioned that intensities of the bands in the encapsulated complexes are very weak in comparison to the corresponding neat complexes due to the low concentration of the complexes in the zeolite matrix. These peaks are similar to those of the free metal complex, which is evidence of the presence of the metal complex entrapped in the zeolite matrix.

The electronic spectra of the encapsulated complexes as well as the ion-exchanged Y-zeolite were recorded in Nujol over the range 200–900 nm as shown in Fig. 2. No absorption bands above 300 nm were observed in the spectra of ion-exchanged-Y zeolites. The light green coloured $[CuL_2(H_2O)_2]$-Y exhibits a broad asymmetric band in the region 600–760 nm ascribed to a d–d transition of an distorted octahedral geometry of Cu(II) ions [38].

The $[FeL_2(H_2O)Cl]$-Y exhibit a weak and broad absorption band centred at 522 nm, which is attributed to d–d transition in the complex and was slightly blue-shifted from their corresponding metal complex bands, suggesting an octahedral geometry around the metal ion [39]. The band due to d–d transitions in Bi(III) base catalysts could not be located in Nujol. All encapsulated complexes exhibit bands between 370 and 387 nm due to symmetry forbidden metal-to-ligand charge-transfer (MLCT) band. Other bands appearing at 310–355, 254–297, 202–221 nm
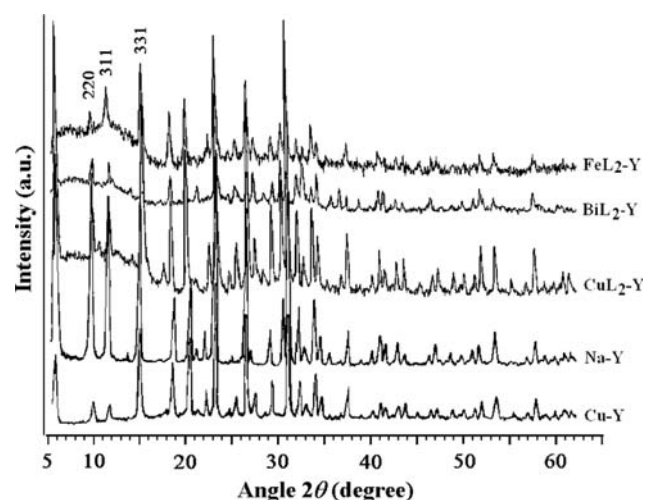
for all complexes arise due to intra-ligand $n-\pi^*$, $\pi-\pi^*$ and $\phi-\phi^*$ transitions, respectively.

The significant alteration in the absorption bands of MLCT and broadening of the $\pi-\pi^*$ transition bands in the encapsulated complexes can be attributed to the interaction between metal complexes and the zeolite framework.
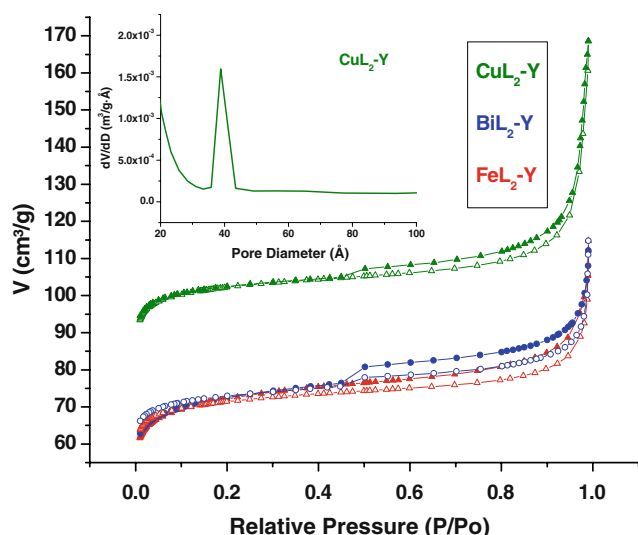
The powder X-ray diffraction (XRD) patterns of zeolite encapsulated complexes show an essentially similar pattern to M–NaY and parent Na–Y zeolite (Fig. 3). These observations indicate that the zeolite framework has not undergone any significant structural change and the crystallinity is retained during the incorporation of the metal and after the encapsulation process.

It has been reported [40, 41] that the relationship between the relative diffraction line intensities of the 220 and 311 reflections in the XRD pattern confirms the formation of a large metal complex ion in the supercage of FAU-type zeolites. It is clear from XRD pattern that the line intensities of the $I220 > I311$ for the Na–Y zeolite, but $I220$ is lower than $I311$ for the encapsulated complexes (Fig. 3). These are clear evidence for the formation of complex ions within the supercage of the zeolite.

After careful comparison of XRD patterns of Na–Y, Cu–Y and $[CuL_2(H_2O)_2]$-Y; new diffraction lines were observed with 2θ value of 25.6 and 46.2° in Cu–Y but not observed in Na–Y. These lines were also observed in $[CuL_2(H_2O)_2]$-Y at the same positions. Also a new line with a 2θ value of 14.2° could be located only in $[CuL_2(H_2O)_2]$-Y. This clearly indicates the insertion of metal complex in the cavities of the zeolite. Location of any new diffraction lines in Fe- and Bi-based catalysts was not possible due to a low intensity and poor resolution of these lines in the XRD pattern, which may attributed to low metal loading.

Catalyst	λ (nm)
$[CuL_2(H_2O)_2]$-Y	202, 221, 272, 297, 320, 352 , 370, 480, 680
$[FeL_2(H_2O)Cl]$-Y	204, 281, 310, 355, 387, 522.
$[BiL_2Cl]$-Y	202, 254, 279, 375

Fig. 2 Electronic spectra and UV–Vis spectral data of the encapsulated complexes

Fig. 3 XRD patterns of Na–Y, Cu–Y and encapsulated metal complexes

Fig. 4 N_2 adsorption/desorption isotherms and pore size distribution of the encapsulated catalysts

Table 2 The textural properties of the encapsulated complexes

Sample	Average pore size (Å)	Pore volume (cm³ g⁻¹)	BET surface area (m² g⁻¹)
Na–Y	24.83	0.34	568
Cu–Y	24.27	0.30	532
$[CuL_2(H_2O)_2]$-Y	24.14	0.21	342
$[FeL_2(H_2O)Cl]$-Y	24.17	0.15	244
$[BiL_2Cl]$-Y	22.98	0.14	240

To study the textural characteristics of the encapsulated complexes in comparison with the parent Na–Y zeolite, nitrogen adsorption–desorption isotherms were recorded. The nitrogen adsorption/desorption isotherms for the parent and the encapsulated complexes zeolites (Fig. 4) are typical type I according to the IUPAC classification [42], which are characteristics of microporous nature of the materials. The representative catalyst $[CuL_2(H_2O)_2]$-Y exhibited narrow BJH pore size distribution curve with less than 4 nm as shown in inset of Fig. 4. Considerable reduction in surface area and micro-pore volume observed for the zeolite-encapsulated complexes from the parent Y-zeolite as shown in Table 2. Since the zeolite crystallinity was retained, the decrease of the surface area and pore volume is interpreted from the presence of complexes in the zeolite nano-cavities and not on the external surface.

The SEM micrographs of Na–Y and zeolite encapsulated metal complexes indicate that there are no changes in the zeolite morphology and structure upon encapsulation of the complexes, which is in agreement with XRD analysis.

The representative images of Na–Y and $[FeL_2(H_2O)Cl]$-Y are reproduced in Fig. 5. Moreover, the SEM images confirmed the absence of extraneous crystals of complex adsorbed on the zeolite surface. In fact, Soxhlet extraction with acetonitrile after encapsulation process serves an excellent solution to remove all the uncomplexed ligand and residual metal complexes physically adsorbed on the external surface of the zeolite.

Thermogravimetric analyses (TGA) data of the encapsulated complexes along with the percent mass loss at different steps and their probable assignments are listed in Table 3 and presented in Fig. 6.

In $[FeL_2(H_2O)Cl]$-Y, the first step occurs at temperature <160 °C with 11 wt% loss due to the presence of trapped water or physically adsorbed water. The second decomposition step at 160–210 °C refer to the loss of intra-zeolite water molecules (3%) i.e. chemisorbed water in the form of OH groups in zeolite Y [43, 44]. The third decomposition step at 210–330 °C losses 1% due to the loss of coordinated water molecule and chloride ion. The rest of the organic ligand decomposes in the final step in a wide range (330–920 °C).

In case of $[BiL_2Cl]$-Y, the third step results of two overlapping steps over a wide range of temperature assigned to the loss of the coordinated chloride ion and the chelating ligand. A very small percent weight loss (2%) in the final step indicates the presence of only small amount of metal complex in the cavity of the zeolite. This is in agreement with the low percent metal content estimated by ICP.

3.2 Molecular Modeling

The molecule encapsulated in a zeolite cage is characterized by steric restriction and may show interesting properties if the size of the molecule is well fitted within the zeolite supercage, which would not be observed under ordinary conditions.

The three-dimensional model structures for the Cu(II), Fe(III) and Bi(III) complexes as well as the ligand were created using HyperChem Version 6.01 molecular modeling to calculate their dimensions using Parametric Method (PM3), performing the semi-empirical Self-Consistent Field (SCF) theory for the geometry optimization are presented in Table 4. The coordination geometry of encapsulated complexes has been obtained with 2:1 ligand to metal stoichiometry analogous to the model complexes by molecular simulations.

Table 4 shows that $[CuL_2(H_2O)_2]$ structure acquires slightly distorted octahedral structure where one of the phenolic oxygen and oxygen of water molecules are in the axial positions and are *trans* to each other with bond

Fig. 5 Scanning electron micrographs of Na–Y (*left*) and [FeL$_2$(H$_2$O)Cl]-Y (*right*)
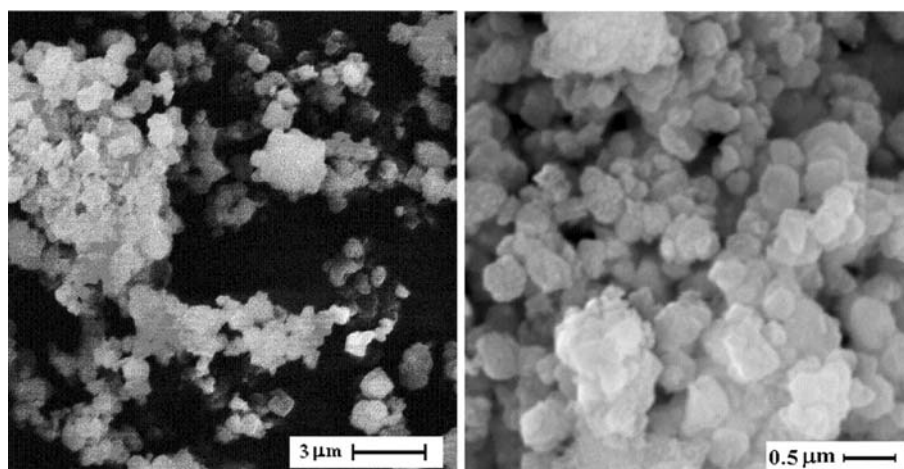
Table 3 Thermal decomposition data for the encapsulated complexes

Catalyst	Temperature range (°C)	Wt loss (%)	Group lost
[CuL$_2$·(2H$_2$O)]-Y	25–170	13	Trapped H$_2$O
	170–280	3	Intra-zeolite H$_2$O
	280–340	2	2H$_2$O (coordinated)
	340–920	12	L
[FeL$_2$(H$_2$O)Cl]-Y	25–160	11	Trapped H$_2$O
	160–210	3	Intra-zeolite H$_2$O
	210–330	1	Cl + H$_2$O (coordinated)
	330–920	5	L
[BiL$_2$Cl]-Y	25–160	8	Trapped H$_2$O
	160–200	1	Intra-zeolite H$_2$O
	200–800	2	L + Cl

L [sal(thiotriazol)] ligand
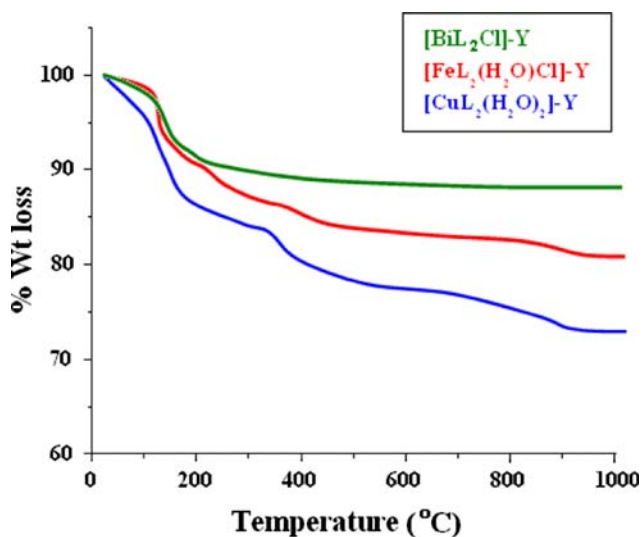
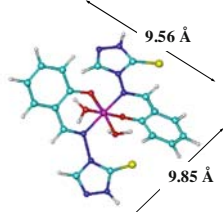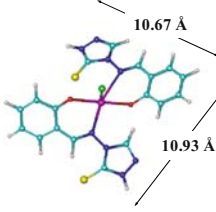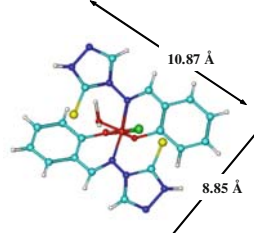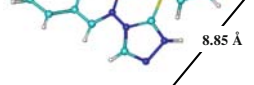**Fig. 6** TGA profile of the encapsulated complexes
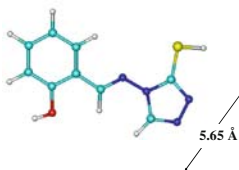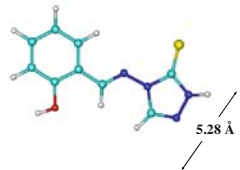
angle of 177.12 Å. Other oxygen and nitrogen of the ligand and oxygen of water molecules are in the equatorial positions.

The 3D optimized geometry shows that the Schiff base ligand is flexible with dimension of 5.28 and 5.65 Å for thione and thiol tautomers, respectively, which is smaller than the pore diameter of Y zeolite and could diffuse freely through the windows (channel openings 7.4 Å) to form complexes inside the supercages with a previously exchanged metal ion that are homogeneously distributed across the zeolite crystals. It can be concluded that these complexes occupies most of the volume of the zeolite-Y supercage (diameter of 12.5 Å), and its size ensures that once the molecules (complexes) are synthesized in the cages, they cannot escape through the window. The resulting complex becomes too large and rigid to escape out of the cages. This confirms that zeolite-Y can accommodate these metal complexes in its supercages without putting any strain.

3.3 Catalytic Activity Studies

Hydroxylation of phenol to two commercially important products, catechol and hydroquinone has been investigated using the encapsulated catalysts in the presence of H$_2$O$_2$ as

Table 4 Dimensions of the optimized geometries

Ligand (Thiol/Thione tautomer)	[CuL$_2$·(H$_2$O)$_2$]	[FeL$_2$(H$_2$O)Cl]	[BiL$_2$Cl]

Table 5 Catalytic activity and selectivity in hydroxylation of phenol over [Cu[sal(thiotriazol)]$_2$·2H$_2$O]-Y] under different reaction conditions

Reaction parameters	Conditions	% Phenol conversion	Selectivity		TOF (h^{-1})[a]
			CAT	HQ	
Reaction temperature (°C)	50	9.3	100	–	213.0
	65	14.3	97.1	2.9	327.6
	80	18.3	94.6	5.4	419.2
Solvent/medium	CH$_3$CN	18.3	94.6	5.4	419.2
	CCl$_4$	4.2	100	–	96.2
	HAc	9.2	100	–	210.8
Amount of catalyst (mg)	5	16.3	98.3	1.7	746.8 (13.9)[b]
	10	18.3	94.6	5.4	419.2 (15.6)
H$_2$O$_2$:Phenol (molar ratio)	25	13.1	100	–	120.0 (11.2)
	2:1	16.3	100	–	373.4 (7.0)[b]
	1:1	18.3	94.6	5.4	419.2 (15.6)
	0.5:1	9.1	100	–	208.5 (15.6)
Phenol:H$_2$O$_2$ (molar ratio)	0.5:1	12.2	100	–	139.7
	1:1	18.3	94.6	5.4	419.2
	2:1	7.3	100	–	334.5
Volume of solvent	2	18.3	94.6	5.4	419.2
	4	10.8	100	–	247.4
	8	6.5	100	–	148.9

[a] *TOF* Turn over frequency: moles of substrate converted per mole of metal (in the solid catalyst) per hour

[b] The data in the parenthesis represent the H$_2$O$_2$ efficiency (%) = (moles of H$_2$O$_2$ utilized in products formation/moles of H$_2$O$_2$ added) × 100

the oxidant. To screen the performances of the encapsulated catalysts, [Cu-[sal(thiotriazol)(H$_2$O)$_2$]-Y catalyst was chosen as the representative catalyst to study the influence of various reaction parameters to acquire maximum hydroxylation.

The influence of reaction temperature on the hydroxylation of phenol over the catalyst is listed in Table 5. To achieve maximum conversion of phenol, the catalytic reactions were carried out at different reaction temperatures, whilst keeping all the other parameters constant. The phenol conversion is doubled on increasing the reaction temperature from 50 to 80 °C with a slight decrease in the selectivity

towards catechol. No further improvement in conversion was achieved at 90 °C due to the faster decomposition of H$_2$O$_2$ itself at high temperature. The catalyst exhibits the highest conversion of phenol after 6 h reaction time at 80 °C, which was selected to carry out the catalytic reactions.

To test the influence of the amount of the catalyst on the catalytic reactivity of phenol hydroxylation, various amounts of catalyst were used and compared. As shown in Table 5, the conversion of phenol increases from 16 to 18% with the increment of the amount of catalyst used from 5 to 10 mg. Further increase in the amount of catalyst to 25 mg, the % phenol conversion and % H$_2$O$_2$ efficiency

decreased to 13.1 and 11.2%, respectively. This is may be due to thermodynamic and mass transfer limitations at higher reaction rates and faster decomposition of H_2O_2 in presence of excess of the catalyst.

Furthermore, high selectivity towards catechol was obtained with molar ratio of catechol to hydroquinone larger than 17 using these amounts of catalyst. Although the phenol conversion decreases with the increasing amount of catalyst (25 mg), the selectivity to catechol reaches 100%, but the TOF value dropped significantly. It could be concluded that the best amount of catalyst used is 10 mg for maximum phenol conversion and high TOF value (419 h^{-1}) after 6 h reaction time.

The activities of hydroxylation in different H_2O_2/phenol molar ratios are studied by varying the amounts of hydrogen peroxide to a fixed amount of phenol and the results are presented in Table 5.

The phenol conversion increased two folds after 6 h reaction time when the molar ratio increased from 0.5:1 to 1:1 and thereafter levelled off after 6 h reaction time. A slight decrease in conversion of phenol was observed when the molar ratio increased from 1:1 to 2:1, however the % H_2O_2 efficiency was markedly decreased to 7 h^{-1}. This may be due to more chemisorption of H_2O_2 and less chemisorption of phenol on the active sites. Nevertheless, no over oxidation product i.e. benzoquinone was detected over all the molar ratios used, although the ring open-pore structure and the channels of Y-zeolites are large enough for all the products to diffuse out easily.

Hence the best molar ratio of H_2O_2/phenol is 1:1. High selectivity to catechol can be obtained at all H_2O_2/phenol molar ratios studied.

The influence of phenol/H_2O_2 molar ratio in phenol conversion was studied with varying amounts of phenol to a fixed amount of hydrogen peroxide. Three different phenol/H_2O_2 molar ratios (0.5:1, 1:1 and 2:1) were used. It is clearly shown that 1:1 phenol/H_2O_2 molar ratio gave the maximum percentage conversion of 18%. On decreasing the molar ratio to 0.5:1 of the substrate/oxidant the over all phenol conversion decreased to 12%. This may be due to the same effect as explained (vide supra). Using 2:1 phenol/H_2O_2 molar ratio i.e. H_2O_2 in half molar amount of phenol, the over all percentage conversion was much lower (7%).

The solvent plays an important and crucial role in catalytic performance as it affects the reaction rates by means of competitive sorption/adsorption phenomenon in the supercages of zeolite, polarity, solvation power and size of the solvent molecule.

To investigate the effect of solvent on the catalytic performance, the solvent was changed from polar solvent, acetonitrile, to non polar solvent, carbon tetrachloride, keeping other reaction conditions constant. Phenol conversion was found to be 18% in acetonitrile, which

decreased markedly on using CCl_4 to 4.2 and 7.1% after 6 and 24 h reaction time respectively. This could be explained by the polarity of the solvent used [45]. Moreover the formation of non-homogeneous (two-phase) system was formed in case of CCl_4, which cause the reaction to occur at the interface, while in acetonitrile the reaction mixture was homogeneous. Similar conclusions were also drawn by our previous reports [18–25].

In terms of selectivity towards catechol and hydroquinone formation both solvents were highly selective to catechol. CCl_4 shows 100% selectivity towards catechol even after 24 h reaction time, whereas in CH_3CN the selectivity was ∼95% after 6 h, which decreased slightly after 24 h reaction time.

On the other hand, the volume of acetonitrile also plays an important role on the percentage conversion. Increasing the volume of solvent used to 4 mL, decrease the catalytic performance to ∼11%. Further increasing in the amount of solvent to 8 mL, the overall percent conversion dropped to 6.5%. This may be attributed to the decrease of reactants concentration in the reaction mixture. With less than 2 mL MeCN or solvent-free the activity showed poor performance due to insufficient amount of solvent to dissolve the reaction mixture to give a homogeneous medium.

The hydroxylation of phenol was also studied in acidic medium (2 mL glacial acetic acid). Acidic medium does not represent a good reaction medium for phenol hydroxylation since, only 9% conversion of phenol was achieved in 6 h. Hydroxylation reaction proceeds unhindered like in presence of CCl_4 but not as in acetonitrile. This may be due to the effect of the acid added decreases the concentration of the intermediate (peroxo species) and in turn the reaction will slow down.

After optimization the reaction conditions for Cu-catalyst, the performances of the Fe- and Bi-encapsulated
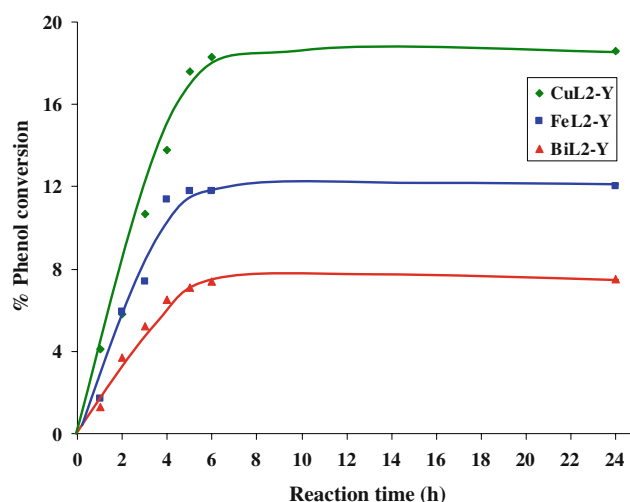

Fig. 7 Catalytic performance of the catalysts with time

catalysts were also studied as a function of time (Fig. 7). The phenol conversion for all catalysts enhanced with reaction time and attains a steady state after ~6 h giving maximum phenol conversion. No significant change in the conversion and selectivity is observed after acquiring a steady state. The Cu-based catalyst shows the highest activity (18%) followed by Fe-catalyst with ~12% conversion of phenol, while Bi-catalyst has the poorest performance (7.4%) after 6 h of reaction time. All the encapsulated catalysts show high selectivity to catechol (>95%) after 6 h reaction time (Fig. 8). Comparing the catalytic activity of our catalysts with other metal encapsulated complexes in zeolite-Y analogues [46–50], our catalysts show lower conversation but superior selectivity towards catechol formation. Compared with TS-2, our catalysts (except Bi-based catalyst) are found to exhibit higher conversion of phenol (11–18 vs. 9.3%) [51], but lower than TS-1 [52–54]. On the other hand $[CuL_2(H_2O)_2]$-Y show comparable activity to that of TS-1 [55] and micro- and nanometer sized TS-1 [56] using acetone as solvent. In general, the selectivity of our catalysts towards catechol formation is superior to that of TS-1 and TS-2.

The stability and reusability was investigated using $[CuL_2(H_2O)_2]$-Y as representative catalyst. The catalyst recovered by filtration and regenerated by Soxhlet extraction (MeCN), dried at 150 °C for 6 h and reused three times. The recovered catalyst then used for the next run under the same reaction conditions. The catalytic result of three successive recycles obtained was almost similar verifying that the catalyst is highly stable and can be reused. This is also confirmed by isolating the catalyst from the reaction mixture after 2 h reaction time and the reaction was continued for another 4 h. It was found that the % conversion remained unchanged without any further

increase which proved that the reaction is catalyzed heterogeneously. The ICP analysis for reaction filtrate shows the absence of metal ions which show that no leaching has occurred during the reaction.

4 Conclusion

It can be concluded that M[sal(thiotriazol)]$_2$ complexes can be encapsulated in Na–Y zeolite supercages without structural modification or loss of crystallinity of the zeolite framework. The physico-chemical studies confirmed the encapsulation of metal complexes in the supercages of zeolite Y. 3D model structure generated for these complexes suggests that zeolite-Y can accommodate these complexes in the FAU supercages without any strain.

The encapsulated metal complexes were tested for hydroxylation of phenol using H_2O_2 as an oxidant which show moderate activity with excellent selectivity towards catechol formation under optimized reactions condition (i.e. 0.05 mol phenol, 1:1 phenol/H_2O_2 molar ratio, 10 mg catalyst, 2 mL CH_3CN at 80 °C). The activity of these catalysts was ordered as follows: Cu > Fe > Bi-based catalysts, which depends on the central metal ion present in the encapsulated complex.

The recovered catalysts after regeneration were reused with no significant loss in the activity was noticed. Comparable IR spectra and XRD images of fresh and used catalysts suggest their further reusability.
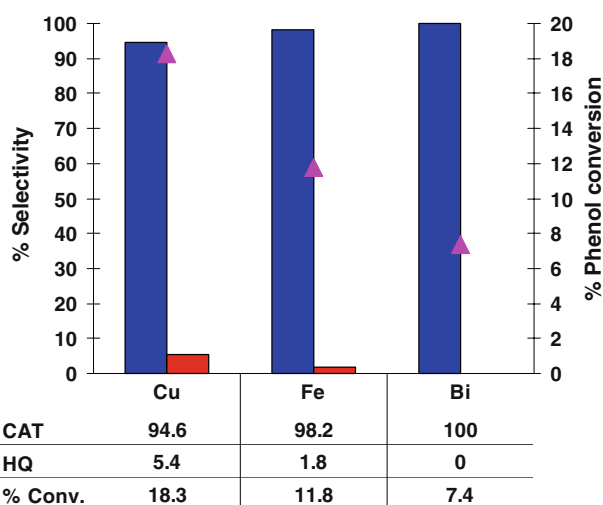
Fig. 8 % Conversion and selectivity for the catalysts. Reaction conditions: PhOH (0.05 mol), H_2O_2 (0.05 mol), catalyst (10 mg), MeCN 2 mL, 6 h at 80 °C

	Cu	Fe	Bi
■ CAT	94.6	98.2	100
■ HQ	5.4	1.8	0
▲ % Conv.	18.3	11.8	7.4

References

1. Parton R, De Vos D, Jacobs PA (1992) In: Derouane EG, Lemos F, Naccache C, Riberio FR (eds) Proceedings of the NATO advanced study institute on zeolite microporous solids: synthesis, structure and reactivity. Kluwer Academic, Dordrecht, 555 pp
2. Knops-Gerrits PP, De Vos D, Thibault-Starzyk F, Jacobs PA (1994) Nature 369:543
3. Grommen R, Manikandan P, Gao Y, Shane T, Shane JJ, Schoonheydt RA, Weckhuysen BM, Goldfarb D (2000) J Am Chem Soc 122:11488
4. De Vos DE, Dams M, Sels BF, Jacobs PA (2002) Chem Rev 102:3615
5. Song CE, Lee S-G (2002) Chem Rev 102:3495
6. Balkus KJ Jr, Gabrielov AG (1995) J Incl Phenom Mol Recognit Chem 21:159
7. Brunel D, Bellocq N, Sutra P, Cauvel A, Lasperas M, Moreau P, Di Renzo F, Galarneau A, Fajula F (1998) Coord Chem Rev 178–180:1085
8. Parton RF, Vankelecom IF, Casselman MJA, Bezoukhanova CP, Uytterhoeven JB, Jacobs PA (1994) Nature 370:541

9. Sabater MJ, Corma A, Domenech A, Fornes V, Garcia H (1997) Chem Commun 1285
10. Piaggio P, McMorn P, Langham C, Bethell D, Page PCB, Hancock FE, Hutchings GJ (1998) New J Chem 22:1167
11. Weitkamp J, Puppe L (1999) In: Catalysis and zeolites: fundamentals and applications. Springer Verlag, Berlin
12. Sheldon RA, van Bekkum H (2001) In: Fine chemicals through heterogeneous catalysis, Wiley-VCH, New York
13. Glaeser R, Weitkamp J (2004) In: The application of zeolites in catalysis. Springer series in Chemical Physics, vol 75 (Basic principles in applied catalysis). Springer Verlag, Berlin
14. Xavier KO, Chacko J, Mohammed Yusuff KK (2004) Appl Catal A 258:251
15. Mukhopadhyay K, Mandale AB, Chaudhari RV (2003) Chem Mater 15:1766
16. Alvaro M, Cardin DJ, Colquhoun HM, Garcia H, Gilbert A, Lay AK, Thorpe JH (2005) Chem Mater 17:2546
17. Ganesan R, Viswanathan B (2004) J Phys Chem B 108:7102
18. Abbo HS, Titinchi SJJ (2009) Appl Catal A 356:167
19. Maurya MR, Titinchi SJJ, Chand S (2004) J Mol Catal A 214:257
20. Maurya MR, Titinchi SJJ, Chand S (2003) J Mol Catal A 201:119
21. Maurya MR, Titinchi SJJ, Chand S (2003) Catal Lett 89:219
22. Maurya MR, Titinchi SJJ, Chand S (2003) J Mol Catal A 193:165
23. Maurya MR, Titinchi SJJ, Chand S (2002) Appl Catal A 228:177
24. Maurya MR, Titinchi SJJ, Chand S, Mishra IM (2002) J Mol Catal A 180:201
25. Maurya MR, Kumar M, Titinchi SJJ, Abbo HS, Chand S (2003) Catal Lett 86:97
26. Burns GR (1968) Inorg Chem 7:227
27. Bala S, Gupta RP, Sachdeva ML, Singh A, Pujari HK (1978) Indian J Chem B 16B:481
28. Jacob CR, Varkey SP, Ratnasamy P (1998) Microporous Mesoporous Mater 22:465
29. Bowers C, Dutta PK (1990) J Catal 122:271
30. Sen AK, Singh G, Singh K, Handa RN, Dubey SN, Squattrito PJ (1998) Proc Indian Acad Sci Chem Sci 110:75
31. McCarrick RM, Eltzroth MJ, Squattrito PJ (2000) Inorg Chim Acta 311:95
32. Escobar-Valderrama JL, Garcia-Tapia JH, Ramirez-Ortiz J, Rosales MJ, Toscano RA, Valdes-Martinez J (1989) Can J Chem 67:198
33. Kajdan TW, Squattrito PJ, Dubey SN (2000) Inorg Chim Acta 300–302:1082
34. Weng NS (1992) Acta Crystallogr C C48:2224
35. Geary WJ (1971) Coord Chem Rev 7:81
36. Shukla PR, Singh VK, Jaiswal AM, Narain G (1983) J Indian Chem Soc 60:321
37. Nakamoto K (1997) In: Infrared and Raman spectra of inorganic and coordination compounds, part I: theory and applications in inorganic chemistry. Wiley, New York
38. Lever ABP (1984) In: Inorganic electronic spectroscopy. Elsevier, New York
39. Srivastava AK, Rana VB, Mohan M (1974) J Inorg Nucl Chem 36:2118
40. Quayle WH, Lunsford JH (1982) Inorg Chem 21:97
41. Quayle WH, Peeters G, De Roy GL, Vansant EF, Lunsford JH (1982) Inorg Chem 21:2226
42. Sing KSW, Everett DH, Haul RAW, Moscou L, Pierotti RA, Rouquerol J, Siemieniewska T (1985) Pure Appl Chem 57:603
43. Meyer G, Woehrle D, Mohl M, Schulz-Ekloff G (1984) Zeolites 4:30
44. Diegruber H, Plath PJ, Schulz-Ekloff G (1984) J Mol Catal 24:115
45. Corma A, Esteve P, Martinez A (1996) J Catal 161:11
46. Salavati-Niasari M, Bazarganipour M (2006) Catal Commun 7:336
47. Maurya MR, Saklani H, Kumar A, Chand S (2004) Catal Lett 93:121
48. Srinivas D, Sivasanker S (2003) Catal Surv Asia 7:121
49. Chavan S, Srinivas D, Ratnasamy P (2000) J Catal 192:286
50. Wilkenhöner U, Langhendries G, van Laar F, Baron GV, Gammon DW, Jacobs PA, van Steen E (2001) J Catal 203:201
51. Reddy JS, Sivasanker S, Ratnasamy P (1992) J Mol Catal 71:373
52. Chao P-Y, Tsai S-T, Tsai T-C, Mao J, Guo X-W (2009) Top Catal 52:185
53. Klaewkla R, Kulprathipanja S, Rangsunvigit P, Rirksomboon T, Nemeth L (2003) Chem Commun 1500
54. Keshavaraja A, Ramaswamy V, Soni HS, Ramaswamy AV, Ratnasamy P (1995) J Catal 157:501
55. Thangaraj A, Kumar R, Ratnasamy P (1991) J Catal 131:294
56. Tsai S-T, Chao P-Y, Tsai T-C, Wang I, Liu X, Guo X-W (2009) Catal Today 148:174